Electrochimica Acta 78 (2012) 212–222

Contents lists available at SciVerse ScienceDirect

Electrochimica Acta

journal homepage: www.elsevier.com/locate/electacta

High performance hybrid supercapacitor based on two nanostructured conducting polymers: Self-doped polyaniline and polypyrrole nanofibers

H.R. Ghenaatian[a], M.F. Mousavi[a,*,1], M.S. Rahmanifar[b]

[a] Department of Chemistry, Tarbiat Modares University, P.O. Box 14115-175, Tehran, Iran
[b] Faculty of Basic Science, Shahed University, Tehran, Iran

ARTICLE INFO

Article history:
Received 26 October 2011
Received in revised form 22 May 2012
Accepted 28 May 2012
Available online 17 June 2012

Keywords:
Hybrid supercapacitor
Self-doped polyaniline nanofiber
Polypyrrole nanofiber

ABSTRACT

A hybrid asymmetric electrochemical supercapacitor is constructed by employing two different nanostructured conducting polymers of polypyrrole (PPy) and self-doped polyaniline (SDPA). Different electrochemical methods, including cyclic voltammetry, galvanostatic charge–discharge and electrochemical impedance spectroscopy (EIS), are performed to characterize the electrochemical performance of the supercapacitor. The maximal working potential window of 1.3 V is associated with more than 97 F g^{-1} of total electrode materials. The cell maintains approximately 70% of its initial capacitance after 1000 cycles with an equivalent series resistance (ESR) below 1.6 Ω cm^2. Furthermore, the system shows high specific energy, specific power and maximum power values of 22.87 Wh kg^{-1}, 570 W kg^{-1} and 45,193 W kg^{-1}, respectively, at a current density of 5 mA cm^{-2} in 1 M KCl. Long-life cycling is achieved by removing dissolved oxygen and using a mild pH electrolyte, which limits the redox activity of the electrically conducting polymers (ECPs). Moreover, the proposed supercapacitor exhibits high capacitance retention of 89% at a higher current density (40 mA cm^{-2}), indicating good electrochemical stability and rate capability. The performance of the proposed hybrid supercapacitor has been compared with two other symmetric cells.

1. Introduction

Nanostructured materials have opened a new opportunity for science and technology [1–4]. Electroactive nanomaterials can improve the performance of electrochemical energy storage systems such as batteries [5] and supercapacitors [6] by allowing for more efficient electrochemical reactions as compared to microstructured materials [7].

An electrochemical capacitor, or "supercapacitor", is considered as one of the important innovations in the field of high power electrical energy storage systems. Supercapacitors can store energy using a single or combination of various charge storage mechanisms, including by the formation of electric double layer (EDL) at electrode–electrolyte interfaces, mainly by using conducting porous materials such as the activated carbon [8] and through a multielectron-transfer Faradaic reaction at or within 2-dimensional surfaces of the electroactive materials such as transition metal oxides [9] and electrically conducting polymers (ECPs) [6]. Toward this end, researchers have made great efforts in developing ECPs as good candidates for supercapacitor electrode materials due to their unique properties such as facile thin film fabrication, ease of processability, light weight and elasticity [10]. According to our survey of the literature, the most common ECPs used in the construction of a supercapacitor are polyindophenine [11], polythiophene [12], p-phenylenevinylene (PPV) [13], polypyrrole (PPy) [14] and polyaniline (PANi) [15–17]. Among these ECP materials, the PANi and the PPy and their derivatives are considered to be the most promising materials for supercapacitor applications due to their high conductivity, fast oxidation-reduction reactions, high energy density, ease of synthesis and low cost [18]. It should be mentioned that, in the construction of supercapacitors, PANi and PPy are used in low and neutral pH electrolyte solutions [19]. Thus, PANi derivatives needed to be active under neutral pH conditions [20]. Among the PANi derivatives, self-doped polyaniline (SDPA) exhibits electrochemical activity over a wide pH range even in neutral and basic solution because of the presence of functional groups carrying negative charge (such as $-COO^-$ and $-SO_3^-$), which act as proton generators and dopants with no need for external ions [21]. In most application, supercapacitors are used to couple with a secondary battery because of their unique properties for delivering high power density together with high energy in a very short time [22], thereby acting as a buffer for high charging–discharging rates.

* Corresponding author. Tel.: +98 21 82883474/82883479; fax: +98 21 82883455.
E-mail addresses: mfmousavi@yahoo.com, mousavim@modares.ac.ir (M.F. Mousavi).
[1] ISE member.

0013-4686/$ – see front matter © 2012 Elsevier Ltd. All rights reserved.
http://dx.doi.org/10.1016/j.electacta.2012.05.139

The specific energy ($W\,kg^{-1}$) of a supercapacitor is given by Eq. (1) [23]:

$$\text{Specific energy (SE)} = \frac{1}{2}C\Delta V^2 = \frac{I\Delta Vt}{2M \times 3600} \quad (1)$$

where C is the specific capacitance ($F\,g^{-1}$), ΔV is the working potential window (V), I is the discharge current density ($A\,cm^{-2}$), t is discharge time (s) and M is the amount of active materials (kg) in the supercapacitor (including positive and negative electrode weight). Based on this equation, two main strategies are envisioned to improve the energy characteristics of supercapacitors: (i) the use of nanomaterials and (ii) increasing working potential window (ΔV).

Nano-sized materials provide not only high surface area but also provide more participation of the electroactive materials in the redox reactions due to rapid ion diffusion into the bulk of nano-sized materials [24]. Thus, application of nanostructured materials could lead to higher specific capacitance [25].

The second strategy for improving the energy characteristic of the supercapacitors is increasing its working potential window [26]. The stability and the nature of the electrolyte and the electroactive materials are the important parameters for determination of a practical operating working potential window for a supercapacitor [27]. The practical working potential window in an aqueous electrolyte is approximately 1 V, whereas in organic electrolytes, it expands to approximately 2.5 V [28]. However, organic solvents suffer serious drawbacks, including low conductivity, which prevents the use of high charge–discharge currents, resulting in a limited power of the supercapacitor, the need for a moisture-free atmosphere and the toxicity characteristics associated with organic systems [29]. Therefore, supercapacitors using aqueous electrolytes would be more attractive. However, it is necessary to find a strategy for increasing the working potential window and the specific energy of these systems through the choice of different materials for the positive and negative electrodes. Also, in comparison with metallic substrates the GO shows the higher electrochemical windows without hydrogen or oxygen evolution in aqueous solution, which allow for supercapacitor operation at the higher possible voltage windows. This appears to be the best solution for increasing the overall working potential window of the supercapacitors [29]. Therefore, it may be possible to obtain both a large electrochemical window and high specific energy density for supercapacitors by choosing some proper electroactive nanostructured materials as positive and negative electrodes.

Various chemical and electrochemical methods have been developed for preparation of nanostructured ECPs [30]. Chemical methods for the fabrication of ECPs typically result in poor contact with the underlying substrate. However, electrochemical polymerization methods provide lower contact resistance between conducting substrate and the deposited ECP. Electrochemical deposition techniques also have more controllability in the resulting structure and conductivity of the ECPs than do the chemical methods [10,31]. Therefore, the best polymerization method for preparation of nanostructured ECPs is a direct synthesis using electrochemical techniques. This allows efficient control of the chemical and physical properties of the ECP films through control of the conditions of the electrochemical deposition.

In continuation of our recent studies on electrical energy storage systems based on SDPA in Zn-PAN batteries [32–37], on the effects of degradation products on OCV of PANi-batteries [38], and, more recently, on SDPA nanofibers as new materials for redox supercapacitors [6] a hybrid supercapacitor based on both PPy and SDPA is assembled in this work to improve the energy characteristics without a decrease in specific capacitance at a mild pH.

2. Experimental

2.1. Materials

High purity grade of *m*-aminobenzoic and pyrrole (98%) were purchased from Aldrich and used as received without further purification. Aniline (Merk) was used after purification by distillation under reduced pressure prior to use. Graphite powders (raw samples) and analytical grade reagents of HCl, KCl, NaH_2PO_4 and Na_2HPO_4 were prepared from Merk or Fluka and used without further purification. All the solutions prepared by using doubly distilled water. During the all experiments, the electrolyte solutions were degassed by pure argon.

2.2. Instrumentation

All electrochemical experiments were carried out by an Autolab General Purpose System PGSTAT 30 (Eco-chemie, Netherlands). A conventional three electrode cell was used in order to electrodeposition of the SDPA and PPy. A GO sheet with 0.5 mm thickness (1 cm × 1 cm) was used as the working electrode, a Pt wire and Ag/AgCl (KCl, saturated) were utilized as the counter and reference electrodes, respectively. Electrochemical investigations of the symmetric and asymmetric supercapacitors were performed using a home-made two electrode cell and the setup was used to monitor the cyclic voltammetry, galvanostatic charge–discharge and EIS (10^5 to 10^{-2} Hz) behavior of the systems. In the symmetric case, two identical SDPA or PPy electrodes were sandwiched using Absorptive Glass Mat (AGM) as a separator in an electrolyte of 1.0 M KCl to construct the supercapacitor. In the hybrid case, the supercapacitor was constructed based on the SDPA as a positive electrode in combination with the PPy as a negative electrode using a same separator and electrolyte.

Morphological investigations of the polymeric films were carried out by using SEM (Philips XL 30).

2.3. Preparation of GO

Before electrodeposition of the PPy and the SDPA, graphite was oxidized to generate oxygenated functionalities, which seem to be beneficial in enhancing the carbon wettability, increasing the substrate surface area, decreasing the interfacial resistance of the substrate/ECP interface and improving the mechanical properties of the substrate [29]. The GO was prepared from natural graphite according to Ref. [39]. At first, raw graphite powder was added gradually to fuming nitric acid with mechanical stirring. Reaction temperature was adjusted at 60 °C, and the graphite was oxidized by stirring with potassium chlorate for 12 h. Finally, the resulting product was centrifuged, and the resulting solid pellet was washed repeatedly with 5% HCl solution and acetone, respectively, and dried in an oven at 60 °C for 12 h. GO powder (60 wt.%) was mixed with 35 wt.% raw graphite powder and 5 wt.% of poly(tetrafluoroethylene) (PTFE). This resulted in a rubber-like paste that was rolled in a film (approximately 3 mm thick) on a flat surface and dried for 12 h at 60 °C. To assure good electrical contact, the electrodes were hot-pressed. The GO plates were activated by immersing in solutions of the monomer and electrolyte for 24 h prior to the electrodeposition.

2.4. Electrodeposition of SDPA and PPy nanofibers

SDPA and the PPy nanofiber films were potentiostatically electrodeposited onto the GO at 0.8 V vs. Ag/AgCl. The SDPA was fabricated from 0.1 M aniline monomer, 0.1 M *m*-aminobenzoic acid and 1 M HCl. Electrodeposition of the PPy was conducted in 0.05 M pyrrole monomer, 0.1 M $LiClO_4$ and 0.2 M phosphate buffer

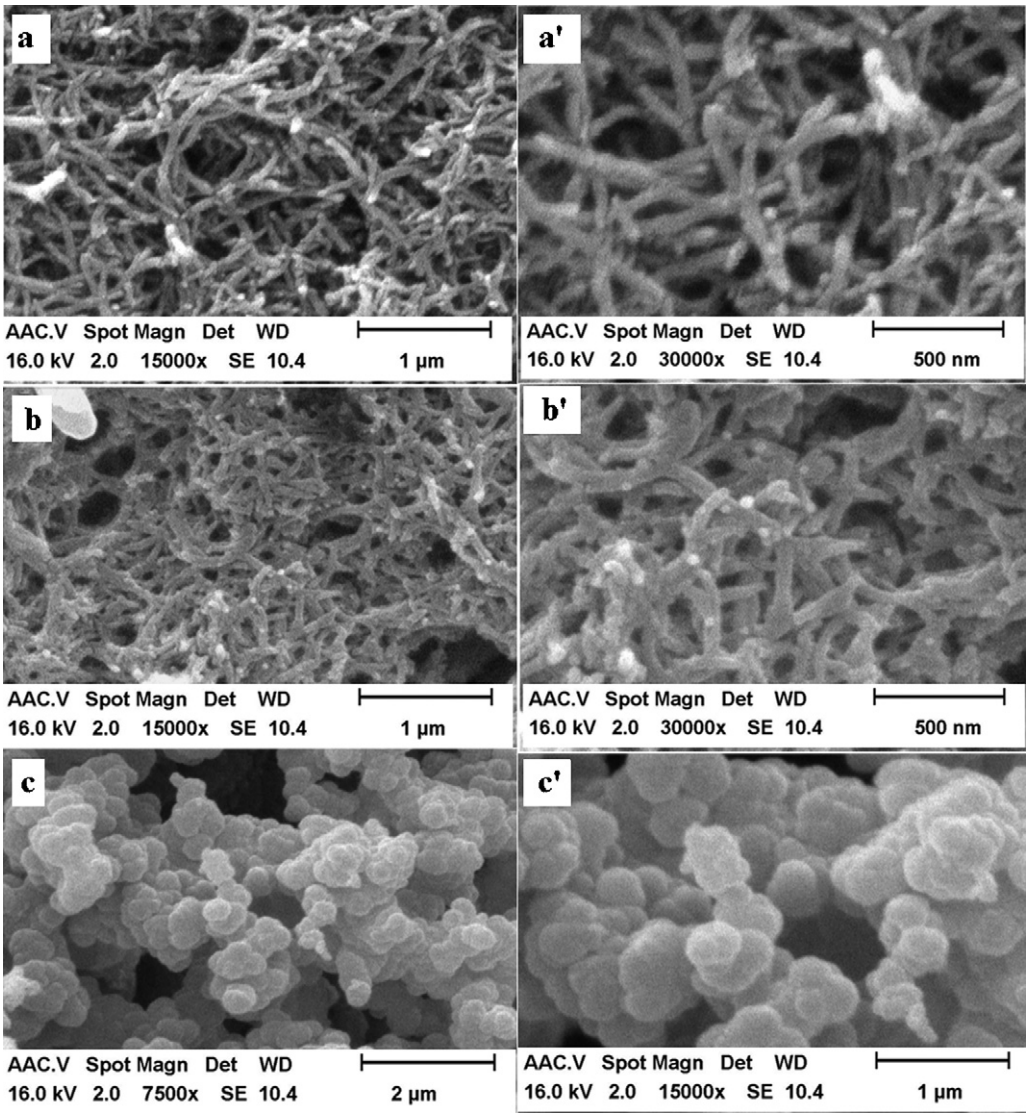

Fig. 1. Scanning electron micrographs of electrodeposited SDPA (a) 15,000× and (a′) 30,000×; PPy synthesized in the presence of PBS as an auxiliary dopant (b) 15,000× and (b′) 30,000×; and PPy synthesized in the absence of PBS as an auxiliary dopant (c) 15,000× and (c′) 30,000× on the GO substrate in a three-electrode cell.

solution (PBS). After electrodeposition of the SDPA and PPy onto the GO, these electrodes were washed 4–5 times with distilled water to remove the remaining monomers. The prepared PPy electrode was immersed in an aqueous solution containing 1 M KCl for 6 h to exchange perchlorate and PBS dopants with chloride.

3. Results and discussion

3.1. SEM studies

SEM experiments were conducted to investigate of the morphology of the PPy and SDPA and the effects of auxiliary dopants (PBS) on the PPy structure. Fig. 1a and a′ shows SEM micrographs of the electrodeposited SDPA at two different magnifications (a) 15,000× and 30,000×. The structure of the prepared film appears to consist of interconnected, uniform nanofibers with no agglomeration and with fiber diameters less than 80 nm. Aniline and *m*-aminobenzoic acid monomers have been previously used to prepare SDPA nanofibers. The presence of the carboxylic acid group in *m*-aminobenzoic acid deactivates its aromatic system with respect to electrophilic substitution due to the electron-withdrawing effect. This electronic effect is also responsible for the higher potential (0.8 V vs. Ag/AgCl) required to oxidize the *m*-aminobenzoic acid monomers, in comparison to aniline alone. Fig. 1b, b′, c and c′ shows SEM images of the electrodeposited PPy with and without PBS as an auxiliary dopant. The PPy electrode prepared in the presence of PBS shows a nanofibrous morphology with fiber diameters less than 70 nm. However, the PPy film in the absence of PBS shows a microgranular morphology (Fig. 1c and c′). These results show the important role of PBS as an auxiliary dopant in the morphology of ECPs. Moreover, in the electrosynthesis of PPy, the morphology is influenced by the nature of the conducting substrate. To prepare PPy nanofibers, a mixture of 1:2 of ClO_4^- and PBS was used for doping, and a GO plate was used as the substrate. GO is a good substrate candidate for electrodeposition of ECPs because of its hydrophilicity due to the presence of oxygenated functionalities, such as epoxide, carboxyl and phenolic groups [29], as shown in Fig. 2. Also, the GO substrate can be cooperatively used with PPy or SDPA to form uniform and adherent films with very low substrate/ECP interfacial contact resistance. Furthermore, this substrate shows the highest electrochemical range without hydrogen or oxygen evolution, in comparison with metallic substrates, which allow for supercapacitor operation at the highest possible working potential window [29]. Fig. 2 shows a schematic representation of

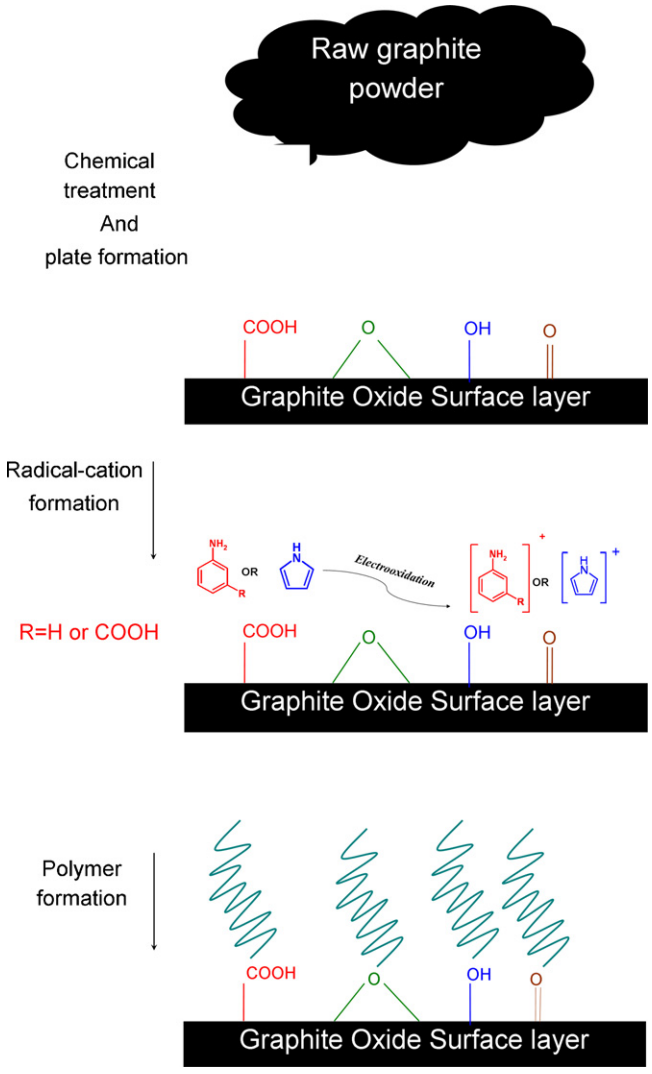

Fig. 2. Schematic representation of the electrochemical formation of PPy and SDPA on the GO electrode.

the procedure used to prepare the PPy and SDPA films on the GO electrode. As is seen in the figure, oxygenated functional groups [40] act as dopants during initial polymer formation and reduce electrical contact resistance between the polymer films and the GO electrode.

3.2. Cyclic voltammetric studies

Cyclic voltammetry was used to study the effect of substrate functionalization, mass tuning of negative and positive poles and to evaluate the performance of the hybrid PPy/SDPA supercapacitor in different working potential windows between 0.0 and 1.5 V.

Fig. 3 shows cyclic voltammograms of raw graphite and GO in 1 M HCl and 1 M KCl electrolytes at a scan rate of 50 mV s^{-1}. The treated graphite (GO) is much more electroactive than the untreated one employed as substrate. GO shows two redox peaks between 0.1 and 0.6 V vs. Ag/AgCl, which exhibits more improvement over graphite. The activity in HCl solution is much greater than what is observed in KCl solution. However, to avoid degradation of the SDPA in acidic media, KCl solutions were deemed suitable for further studies. The observed redox peaks are due to the transition between the quinone and hydroquinone states, which is typical for carbon materials with oxygen-containing functionalities, as reported by others [40].

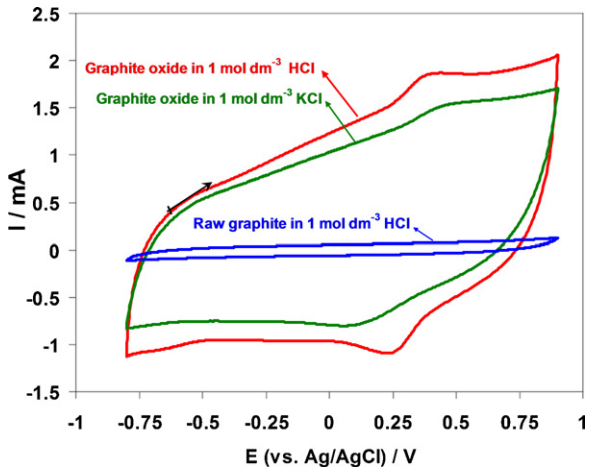

Fig. 3. Comparative cyclic voltammograms of raw graphite and GO in two different electrolyte solutions, 1 M HCl and 1 M KCl, at a scan rate of 50 mV s^{-1} in a three-electrode cell.

To evaluate the applicability of PPy and SDPA in hybrid supercapacitor as the negative and the positive electrodes, respectively, their cyclic voltammograms were separately recorded. Fig. 4 shows the cyclic voltammograms of PPy and SDPA electrodes in a three electrode cell with potential ranges of −0.7 to 0.3 V and −0.2 to 0.8 V vs. Ag/AgCl, respectively, at a scan rate of 20 mV s^{-1} in 1 M KCl electrolyte. The CVs of the PPy and SDPA electrodes show distinguishable coupled peaks that correspond to the conversion between the different redox states of these two ECPs. During the charging process of the hybrid supercapacitor, the potential of the electrodes will be split depending on their individual capacitances. As is shown in Fig. 4, SDPA shows two pairs of peaks that are related to leucoemeraldine/emeraldine and emeraldine/pernigraniline conversion. In comparison with emeraldine, leucoemeraldine and pernigraniline are poor conductors. Also, PPy shows a pair of redox peaks related to transition between its accessible redox states (Fig. 4). At the fully reduced state, it is undoped and its conductivity is greatly decreased, resulting in the formation of an insulating material. Moreover, the high background current observed in these CVs clearly shows evidence of a non-Faradaic mechanism for electrical energy storage.

Therefore, at a working potential window beyond the fully charged state of the hybrid PPy/SDPA supercapacitor, the SDPA will be irreversibly oxidized and the PPy fully reduced, which would result in a marked reduction in the supercapacitor performance, as has been reported by others [41].

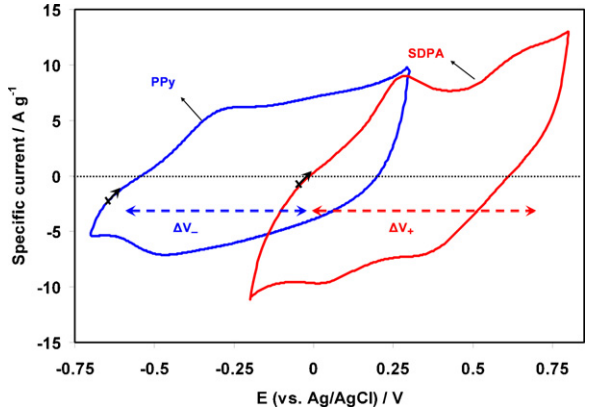

Fig. 4. Comparative cyclic voltammograms of PPy and SDPA in a three-electrode system in 1 M KCl aqueous solution at a scan rate of 20 mV s^{-1}.

To use the CV data in the calculation of specific capacitance for the PPy and SDPA electrodes to obtain the highest cell working potential window, mass tuning of the negative and positive electrodes should be conducted [42] because the specific capacitance of the SDPA and the PPy electrodes is highly dependent on a variety of parameters, including the charge–discharge current density and potential variation, type of electrolyte and solvent, nature of the substrate, and thickness of the electroactive materials on the substrate [41]. Therefore, to ensure that the hybrid PPy/SDPA supercapacitor operates over the highest range of working potential window, it is necessary to tune the weight ratio of the SDPA and the PPy electrodes. To tune the positive/negative weight ratio, it should be ensured that the voltammetric charges of the SDPA (Q_+) and the PPy (Q_-) electrodes are balanced ($Q_+ = Q_-$). The voltammetric charges (Q_{ECP}) were calculated based on the following equations [42]:

$$Q_{ECP} = C_{single} \times \Delta V \times m \quad (2)$$

where ΔV is an effective potential window (V), m is mass of the ECP electrodeposited on the GO electrode (g) and C_{single} is specific capacitances ($F\,g^{-1}$) of each ECP electrode in the three electrode system. C_{single} was calculated based on the cyclic voltammograms (Fig. 4) using Eq. (3) [43,44]:

$$C_{single} = \frac{\int IdV}{sm\Delta V} \quad (3)$$

where I is the cathodic response current (A), s is the potential scan rate ($V\,s^{-1}$), ΔV potential variation range (V) and m is the amount of active material (g). In this equation, term of $\int IdV$ is the area under the cyclic voltammogram in cathodic peak with dimension of "Volt Amper". Dividing the integral over the potential range (ΔV), it results in average voltammetric current ($I_{ave} = (\int IdV)/\Delta V$). So based on the following equation specific capacitance of the electrodes can be calculated.

$$C_{single} = \frac{I_{ave}}{sm} \quad (4)$$

Based on Eq. (4), a specific capacitance of 410 $F\,g^{-1}$ and 365 $F\,g^{-1}$ was calculated for SDPA and PPy electrodes, respectively. According to Eq. (2), to obtain $Q_+ = Q_-$, the mass balance will require [45]:

$$\frac{m_+}{m_-} = \frac{C_- \times \Delta E_-}{C_+ \times \Delta E_+} \quad (5)$$

Therefore, the weight ratio m_{SDPA}/m_{PPy} was chosen to be approximately 0.9. As a result, the PPy and SDPA electrodes should be reversibly charged across their stable forms over different potential ranges because the two materials have different characteristic, and at this weight ratio, it is expected that the proposed PPy/SDPA supercapacitor would operate at a higher working potential window (1.5 V) compared to the maximum 0.8 V for the individual; symmetric cell configurations (PPy/PPy and SDPA/SDPA).

The cyclic voltammetric study was also conducted across a wide working potential window of 0.0–1.5 V to evaluate both the Faradaic and non-Faradaic charge storage mechanisms and to determine a suitable operating working potential window for the hybrid PPy/SDPA supercapacitor. Fig. 5 shows the cyclic voltammetric responses of the PPy/SDPA system at an optimal electrode mass ratio of 0.9 and at a scan rate of 20 mV s^{-1} in 1 M KCl electrolyte. The observed quasi-rectangular shape of the CV curves (Fig. 5) suggests that the hybrid PPy/SDPA supercapacitor exhibits capacitive behavior over a large working potential window. The hybrid PPy/SDPA system is able to store energy by two mechanisms. First, by a double layer mechanism based on accumulation of charge at the ECPs/electrolyte interfaces in the low working potential window according to:

$$(ECPs)_{surface} + A^- - e^- \leftrightarrow ([ECPs]^+//A^-)_{surface} \quad (6)$$

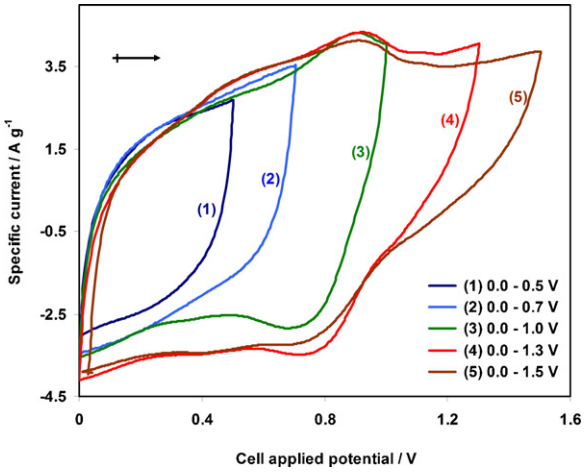

Fig. 5. Cyclic voltammograms of the optimized hybrid PPy/SDPA supercapacitor at different working potential windows at a scan rate of 20 mV s^{-1} in 1 M KCl. The mass of PPy and SDPA electrodes are 3 and 2.7 mg, respectively.

in which the potentials at the negative and positive electrodes are insufficient to allow for the redox reactions [46]. The second mechanism is the Faradaic mechanism based on the redox processes at the ECPs (pseudocapacitance) in the high working potential window as shown in Eq. (7), where A^- refers to the dopants.

$$(ECPs) + A^- - e^- \leftrightarrow ([ECPs]^+A^-)(doping/dedoping) \quad (7)$$

Thus, when the working potential window is 0.0–0.5 and 0.0–0.7 V, only the electric double layer mechanism is operative. By increasing the working potential window to 1 V, the oxidation/reduction peaks appear in the charging–discharging branch, and the behavior of the hybrid PPy/SDPA supercapacitor deviates slightly from the ideal rectangular shape due to the presence of two redox couples, which are indicative of the pseudocapacitance properties that imply onset of the Faradaic redox reactions at the PPy and SDPA electrodes [46]. Increasing the working potential window to 1.3 V results in a significant increase in the anodic and cathodic current, suggesting the occurrence of redox reactions on the PPy and SDPA electrodes. These Faradaic reactions are electrochemically stable at this operating potential window. Increasing the working potential window of the cell to 1.5 V results in a decrease in the anodic and cathodic current due to dedope of the PPy and polyaniline degradation also the irreversible conversion of emeraldine to pernigraniline.

The specific capacitance of either symmetric or asymmetric supercapacitors were calculated according to Eq. (4), replacing m with M (total mass) as shown in Eq. (10) [44] where M is the amount of active material (g) in the supercapacitor (both positive and negative electrodes). The specific capacitances of the hybrid PPy/SDPA supercapacitor in the different working potential window were calculated using Eq. (10) with data from the cyclic voltammograms (Fig. 5), as summarized in Table 1. The maximum specific capacitance of the hybrid cell was obtained at 1.3 V. By increasing the working potential window to 0.7 V, a charge storage mechanism based on formation of the EDL prevailed. However, increasing the applied working potential window to 1.3 V allows both EDL formation and Faradaic redox reactions to contribute to electric energy

Table 1
The specific capacitance of the hybrid supercapacitor PPy/SDPA at different working potential window (V) evaluated from CV test.

Working potential window (V)	0.0–0.5	0.0–0.7	0.0–1.0	0.0–1.3	0.0–1.5
Specific capacitance ($F\,g^{-1}$)	81	83	92	97	90

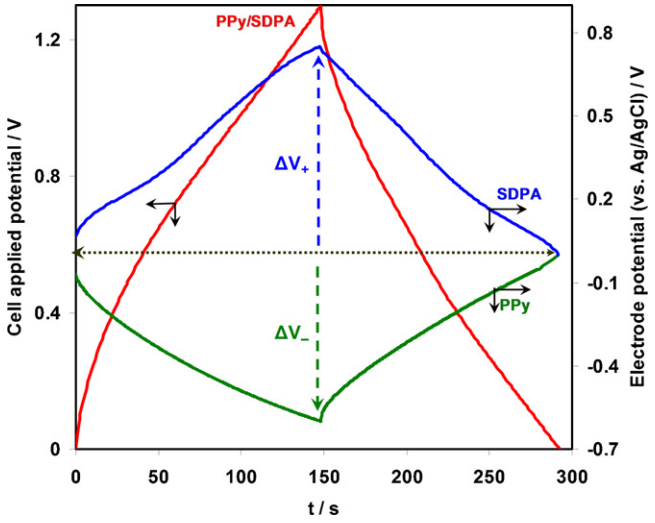

Fig. 6. working potential window–time curve for the hybrid PPy/SDPA supercapacitor and potential–time for the individual electrodes vs. Ag/AgCl at a constant charge–discharge current density of 5 mA cm^{-2} in 1 M KCl aqueous solution.

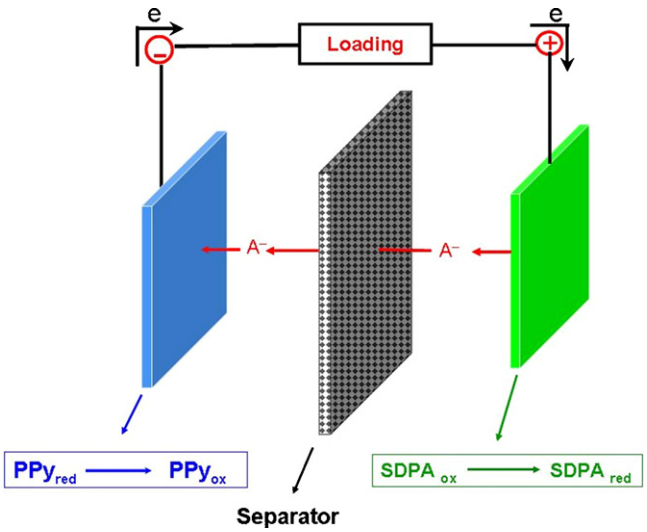

Fig. 7. Schematic view of the hybrid PPy/SDPA supercapacitor with SDPA as the positive electrode, PPy as the negative electrode and AGM as a separator.

storage; above this cell potential window, the SDPA undergoes an irreversible chemical reaction, resulting in the degradation of the active materials. Also, at higher working potential window than 1.3 V, the PPy is dedoped and the SDPA is fully oxidized that caused the PPy/SDPA work at poor performance. Then, by increasing the maximum working potential window up to 1.3 V results show better performance and more potential increasing lead to a decrement in the supercapacitor performance.

3.3. Galvanostatic charge–discharge investigation

Galvanostatic charge/discharge experiments were considered to evaluate the electrochemical performance of the hybrid PPy/SDPA supercapacitor. The potential variations for single electrodes were separately recorded when an Ag/AgCl reference electrode is added to ensure that the hybrid system can operate at the highest possible working potential window.

Fig. 6 shows both the potential-time profiles of the individual electrodes vs. Ag/AgCl and the working potential window–time curves of the hybrid PPy/SDPA supercapacitor at a constant current density of 5 mA cm^{-2} in KCl solution. For recording the potential variation of the PPy and the SDPA electrodes, the equilibrium potential was placed at 0.0 V vs. Ag/AgCl. When the hybrid PPy/SDPA supercapacitor is charged from 0.0 to 1.3 V, the potential varies between 0.0 V and 0.7 V vs. Ag/AgCl for the SDPA electrode and between 0.0 V and −0.6 V vs. Ag/AgCl for the PPy electrode. As shown in Fig. 6, the potential variations are almost sloping with one and two steps for the negative and positive electrodes, respectively, which agree with the CV results (Fig. 4). This is attributed to the potential-dependent nature of Faradaic redox reactions. The PPy and the SDPA are p-doped polymers (anion-inserting polymers). This means that upon extraction of the electrons from a neutral segment of their quinoid chains, some local positive charge deformation occurs, creating a polaron. If the oxidation process continues further, more electrons have to be removed from the electrodes, resulting in the formation of cation radicals, or bipolarons, which are energetically preferred to the formation of two separate polarons. If the weight ratio m_{SDPA}/m_{PPy} is not exactly tuned, during the charging process, the oxidation and reduction of the SDPA and the PPy electrodes, respectively, would not be complete, and the hybrid system would operate at a lower working potential window than expected [22]. However, during the charge/discharge processes (Fig. 6), both the PPy and the SDPA electrodes operate reasonably over the expected potential ranges and the hybrid PPy/SDPA supercapacitor can operate at the working potential window 1.3 V.

Fig. 7 shows schematically how the PPy and the SDPA electrodes operate in the hybrid supercapacitor assembly. When the hybrid PPy/SDPA supercapacitor is loaded (discharge process), the stored electrical energy is depleted by the interaction between the PPy, the SDPA and the electrolyte. The total cell reaction is:

$$\text{Negative}: \mathrm{PPy_{red}} + n\mathrm{Cl^-} \overset{\text{Discharge}}{\longrightarrow} \mathrm{PPy_{ox}} + ne \quad (8)$$

$$\text{Positive}: \mathrm{SDPA_{ox}} + ne \overset{\text{Discharge}}{\longrightarrow} \mathrm{SDPA_{red}} + m\mathrm{Cl^-} \quad (9)$$

In this process, the PPy electrode is oxidized and releases electrons to the current collector (GO) and the electrons are transported to the positive SDPA electrode via an external circuit for the cathodic reaction. Parallel to the above chemical reaction, the SDPA electrode is reduced and becomes more negative (anodic reaction). According to the charge neutrality, the anions (Cl^-) flow to the negative PPy electrode. It should be mentioned that the SDPA has the functional groups with negative charge (—COO^-), which partially eliminates the ion mobility problem. Therefore, it is not necessary to eject n electrons to maintain electroneutrality if n anions enter the scheme as dopants.

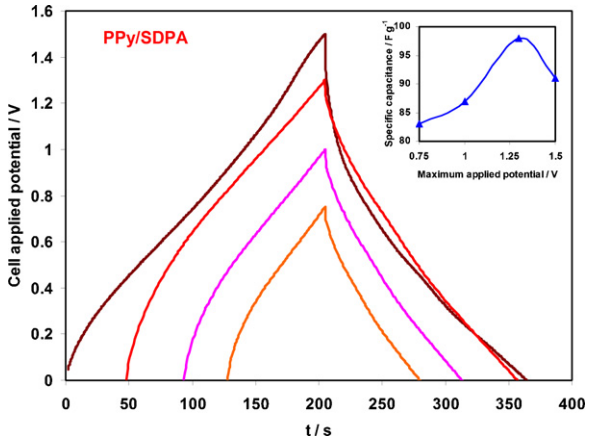

Fig. 8. Galvanostatic charge–discharge profiles of the hybrid PPy/SDPA supercapacitor at different maximum working potential windows with a current density of 5 mA cm^{-2} in 1 M KCl.

Table 2
The specific capacitance of the hybrid supercapacitor PPy/SDPA at different working potential window (V) evaluated from galvanoststic charge–discharge test.

Working potential window (V)	0.0–0.75	0.0–1.0	0.0–1.3	0.0–1.5
Specific capacitance ($F g^{-1}$)	83	87	98	91

Fig. 8 shows the galvanostatic charge–discharge profiles of the hybrid system at four different maximum working potential windows of 0.75, 1.0, 1.3 and 1.5 V. Increasing the working potential window results in an increase of the charge–discharge times with a columbic efficiency of approximately 95% up to 1.3 V. Increasing the maximum working potential window to 1.5 V results in a drop in the columbic efficiency to approximately 90%. The specific capacitance ($F g^{-1}$) of the hybrid cell was calculated using Eq. (10), and is shown as an inset in Fig. 8 and Table 2:

$$\text{Specific capacitance} = \frac{It}{\Delta V M} \tag{10}$$

where I denotes the applied constant discharge current (A), t is the discharge time (s) and ΔV is the discharge working potential window (V) [47]. The specific capacitance increased to an applied potential window of 1.3 V with a highest value of 98 $F g^{-1}$, and it decreased at the higher working potential window of 1.5 V (91 $F g^{-1}$). The drop in specific capacitance is likely due to irreversible reactions and more degradation of the PPy and SDPA electrodes at this working potential window.

Fig. 9a–c shows galvanostatic charge/discharge profiles of the two symmetric supercapacitors, PPy/PPy and SDPA/SDPA, and the hybrid cell PPy/SDPA, respectively, at constant current densities of 5–40 mA cm^{-2} in 1 M KCl electrolyte solution. The calculated specific capacitance of the symmetric systems at a current density of 5 mA g^{-1} using Eq. (10) shows values 91 and 102 $F g^{-1}$ for the PPy/PPy and the SDPA/SDPA cells, respectively. As can be seen in Table 2, the specific capacitance of the hybrid PPy/SDPA cell at 1.3 V is 98 $F g^{-1}$, which is comparable with the values of the specific capacitance for the symmetric supercapacitors.

3.4. Performance of hybrid supercapacitor PPy/SDPA

ESR analyses of the PPy/PPy, SDPA/SDPA and hybrid PPy/SDPA cells were also calculated using the charge–discharge profiles of Fig. 9a–c. The output potential window dropped sharply at the beginning of each experiment, proportional to the ESR of the systems. The ESR (Ω) could be calculated according to Eq. (11):

$$\text{ESR} = \frac{(E_{\text{Charge}} - E_{\text{Discharge}})}{2I} \tag{11}$$

where I, E_{charge} and $E_{\text{discharge}}$ are the applied constant discharge current (A), the output potential window of the cell at the end of charge and at the beginning of discharge after the Ohmic drop (V), respectively [48]. This gives average values of 1.8, 1.5 and 1.6 (Ω) for the two symmetric supercapacitors and the hybrid supercapacitor, respectively, at constant charge–discharge current density of 5 mA cm^{-2}. These low internal resistance values confirm that these systems were properly assembled.

The maximum power (P_{max}) (W kg^{-1}) accessible by the assembled cells was calculated according to Eq. (12) [49] based on Fig. 9a–c.

$$\text{Maximum power} = \frac{E^2_{\text{Discharge}}}{4\text{ESR}M} \tag{12}$$

where these parameters were introduced previously. Based on this equation, the values 14,155, 19,019 and 45,193 W kg^{-1} were obtained for the symmetric PPy/PPy and SDPA/SDPA supercapacitors and the hybrid PPy/SDPA supercapacitor, respectively. The comparison of the P_{max} of these three systems shows the advantage of the hybrid supercapacitor, which shows an improvement of more than 3 times relative to the PPy/PPy supercapacitor and an improvement of more than 2 times relative to the SDPA/SDPA supercapacitor. The comparison of P_{max} for the two symmetric cells shows a higher value for the SDPA/SDPA cell as compared to the PPy/PPy system due to the participation of functional groups with negative charge (—COO^-) in the SDPA system, which decrease the ion mobility limitations during the charge–discharge process.

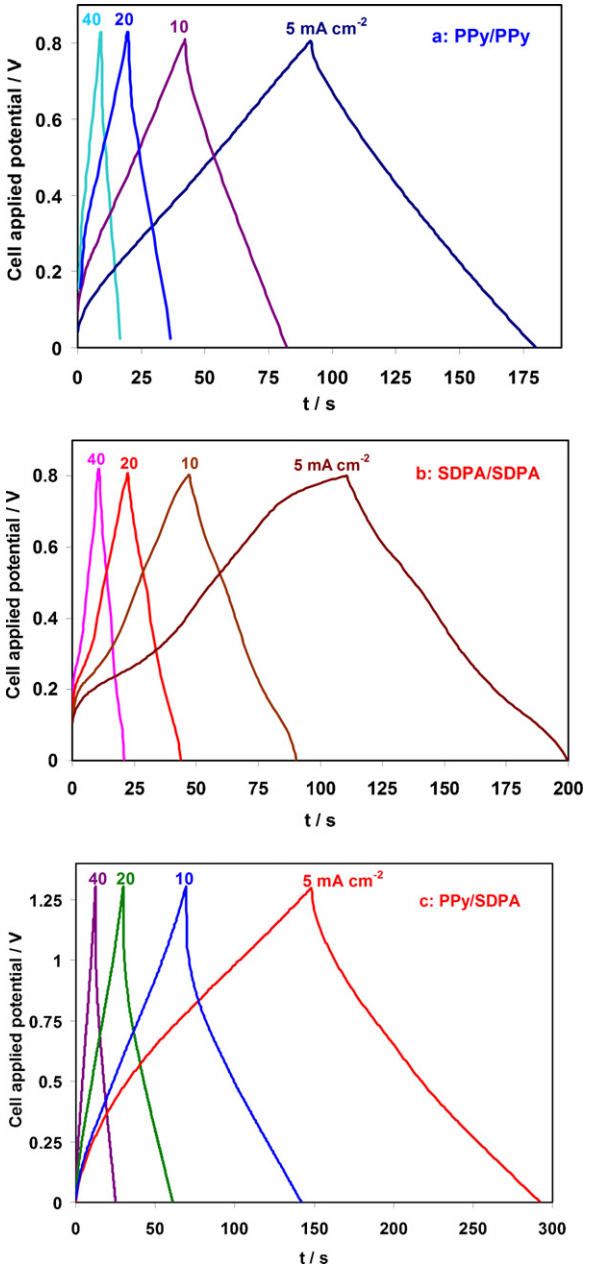

Fig. 9. Galvanostatic charge–discharge curves for the symmetric PPy/PPy and SDPA/SDPA supercapacitors and the hybrid PPy/SDPA cell at constant current densities of 5–40 mA cm^{-2} in 1 M KCl electrolyte solution.

The Ragon plots for the hybrid and symmetric systems calculated from the results of the galvanostatic discharge curves (Fig. 9a–c), based on Eqs. (1) and (13) at different current densities from 5 to 40 mA cm^{-2}, as shown in Fig. 10.

$$\text{Specific power} = \frac{I\Delta V}{2M} \tag{13}$$

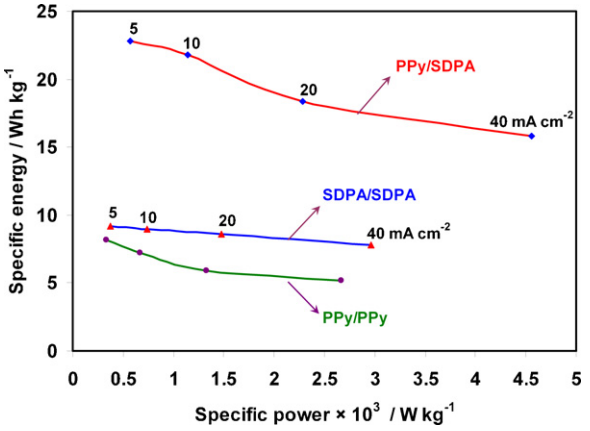

Fig. 10. Ragon plots of the symmetric PPy/PPy and SDPA/SDPA supercapacitors and the hybrid PPy/SDPA cell at different discharge current densities from 5 to 40 mA cm^{-2}.

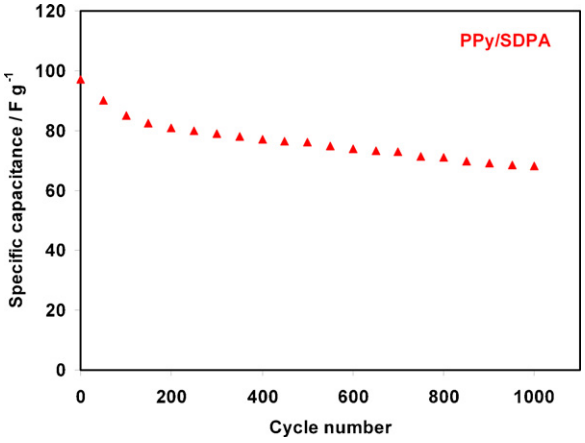

Fig. 12. Dependence of the specific capacitance of the hybrid PPy/SDPA supercapacitor on cycle number at a charge–discharge current density of 5 mA cm^{-2}.

Fig. 10a–c shows that the hybrid PPy/SDPA supercapacitor exhibits outstanding performance due to the expanded working potential range (1.3 V against 0.8 V) compared to two other systems. Higher performance of the SDPA/SDPA (Fig. 10b) than PPy/PPy (Fig. 10c) in the same potential range of 0.8 V can be attributed to the presence of the dopant groups. For example, at a constant current density of 5 mA cm^{-2}, the best specific energy of 22.87 W kg^{-1} was obtained at a corresponding specific power of 570 W kg^{-1} for the hybrid cell, whereas specific energies of 8.3 and 9.15 W kg^{-1} were obtained for the PPy/PPy and SDPA/SDPA symmetric configurations, respectively. The specific energy and specific power are significantly enhanced upon raising the working potential window of the hybrid cell. As a result, the best way to increase the specific energy at a constant specific capacitance of the ECP-based supercapacitors is the application of ECPs with different operating potentials for the negative and positive electrodes.

Another useful parameter used to evaluate supercapacitor performance is high-rate dischargeability (HRD), which shows the power properties of the system during the discharge process. Fig. 11 shows the HRD of both symmetric PPy/PPy and SDPA/SDPA supercapacitors and the hybrid PPy/SDPA supercapacitor, which were calculated based on Fig. 9a–c according to Eq. (14):

$$\mathrm{HRD}(\%) = \frac{C_d}{C_1} \times 100 \tag{14}$$

where C_d is the discharge capacity of the hybrid PPy/SDPA supercapacitor at a certain current density and C_1 is the discharge capacity at 5 mA cm^{-2} [50]. At the high discharge current density of 40 mA cm^{-2}, the SDPA/SDPA and the hybrid PPy/SDPA cells exhibit better performance than the PPy/PPy. This can be attributed to the fact that as much as the internal functional groups with negative charge (—COO$^-$) in the SDPA material present, the need to external dopant will be decreased. Being provided by the internal dopants during the charge–discharge processes, higher power characteristic is observed. Cycling performance for the hybrid PPy/SDPA supercapacitor at a working potential window of 1.3 V was evaluated at 5 mA g^{-1} for 1000 continuous cycles, as shown in Fig. 12. The specific capacitance decreased by only 30% after 1000 cycles. Although the presented system has more specific energy and power compared to the commercial cases [51], but more study on its cycle performance is still needed. This modest decrease of the capacitance suggests good cycle stability for the hybrid cell, which can be reasonably attributed to removing dissolved oxygen and using a mild pH electrolyte, which prevents high rate degradation of these ECPs.

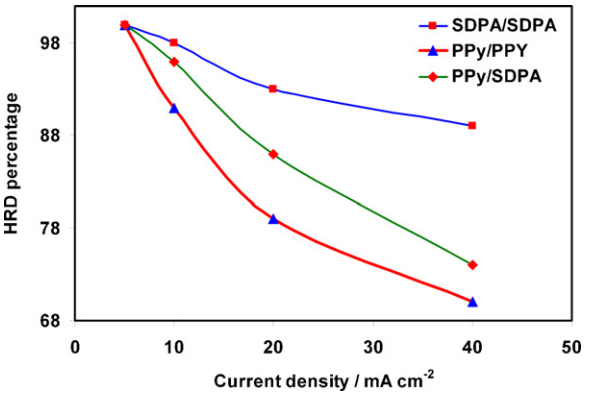

Fig. 11. Relationship between the high rate dischargeability and discharge current density for the three different systems: PPy/PPy, SDPA/SDPA and PPy/SDPA.

3.5. EIS studies

EIS was also used to evaluate the supercapacitor performance and to study the electrochemical behavior of the hybrid and symmetric supercapacitors. Recording the EIS plots at different applied potential windows of the cells (0.0–0.8 V for both symmetric cells and 0.0–1.5 V for hybrid cell) over a frequency range of 10^5 to 10^{-2} Hz led to further clarification of the system behavior (Fig. 13a, and S1 and S2, supplementary material).

In both the symmetric and hybrid cells, Nyquist plots show semicircles in the low and high frequency ranges with a change in diameter upon increasing the applied potential window. As can be seen from the point of intersection at a high frequency with the real axis, the internal resistances of the supercapacitors are below 2 Ω in agreement with results obtained from the charge–discharge experiments. For the quantitative evaluation of different parameters of the both symmetric and hybrid supercapacitors, the experimental data were fitted to the equivalent circuit model (Fig. 13b). In the circuit parameters, R_s, R_{ct1}, R_{ct2}, CPE_1 and CPE_2 are the solution resistance, ionic charge-transfer resistance, Faradaic charge-transfer resistance, double layer capacitance, and bulk Faradaic pseudocapacitance, respectively. The CPE is obtained by:

$$Z_{CPE} = T_{CPE}(j\omega)^{-n}_{CPE} \tag{15}$$

where T and n are the CPE coefficient and exponent, respectively, and ω is the angular frequency. The values for n are in the range between −1 and 1. In the case of $n = -1$ the CPE is equivalent to

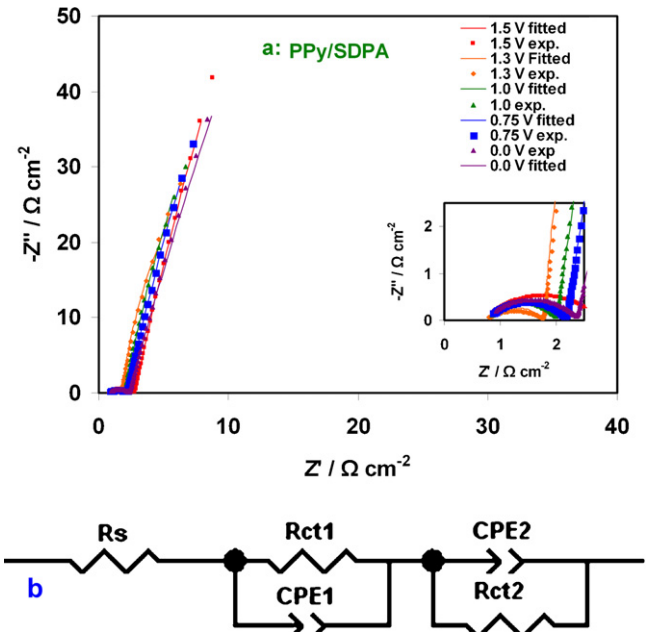

Fig. 13. Nyquist plots of the hybrid PPy/SDPA (a) supercapacitors at different applied potential windows in 1 M KCl. Equivalent circuit model used for fitting of experimental data (b). The solid lines represent the fitting results.

a pure inductor, for $n = 0$, the CPE is equivalent to a pure resistor, $n = 0.5$ denotes diffusion behavior and at $n = 1$, the CPE is equivalent to a pure capacitor [52].

Table 3 shows the results of fitting the EIS data at different applied potential windows. The R_{ct1} in all cases is lower (approximately 10^3 times) than the R_{ct2}, which suggests a higher rate of energy storage by the electrically double layer formation as compared to the Faradaic reactions. R_{ct1} and R_{ct2} decrease with increasing applied potential window for both the symmetric cells up to 100%. However, in the hybrid PPy/SDPA supercapacitor, decreases in R_{ct1} and R_{ct2} are observed up to an applied potential window 1.3 V, due to the greater contribution of physical (double layer) and electrochemical phenomena. The comparison of R_{ct1} (ion transfer resistance) with R_{ct2} (electron transfer resistance) shows a decrease of the charge transfer resistance for R_{ct2} less than R_{ct1}. However, at an applied potential window of 1.5 V, an increase in the R_{ct1} and R_{ct2} values is observed due to the fact that the PPy electrode is fully dedoped and the SDPA electrode is over-oxidized.

The C_2 and C_1 increase with increasing applied potential window for both symmetric PPy/PPy and SDPA/SDPA cells up to 75%. However, in the hybrid PPy/SDPA supercapacitor, increases of the C_1 and C_2 are observed up to an applied potential window of 1.3 V. However, at an applied potential window of 1.5 V, the values of C_1 and C_2 decrease due to full dopant loss and oxidation of the PPy and the SDPA electrodes, respectively. A comparison of all obtained C_1 and C_2 values shows higher values of the C_2 (approximately 100 times) than the C_1, which demonstrates a greater contribution of the Faradaic reactions as compared with the physical phenomena (double layer). Internal dopants can reduce the need to external dopants that this phenomenon can interestingly play two different roles, one decreasing the double layer capacitance, and another facilitating the redox reactions in the SDPA structure. It can be seen that the EIS can completely show this dual role, determining the contributions of double layer capacitance and Faradaic capacitance. Accordingly, the lower values of the C_1 for the SDPA/SDPA system at the same applied potential window than for the PPy/PPy system (Table 3) can be attributed to the participation of internal functional groups with negative charge (—COO^-) in the SDPA electrodes. As the charges are compensated by the internal dopants, fewer numbers of diffused external dopants lead to lower charge storage as electrical double layer capacitances, resulting in lower values for C_1 for the SDPA compared to PPy. However, these internal dopants can still facilitate the Faradaic reactions in SDPA which result in higher values of C_2 compared to that of PPy. Overall, Faradaic reactions play a dominant role due to the higher contribution (100 times greater than non-Faradaic) in charge storage. This is in good agreement with the obtained results using charge/discharge measurements (Fig. 9).

The maximum specific capacitance is observed at 0.8 V for both symmetric supercapacitors and is observed at 1.3 V for the hybrid cell.

To further explore the capacitance behavior of the systems, differential capacitance (C_t) values were calculated, based on Eq. (16) [53]:

$$Z'' = \frac{1}{2\pi C_t f} \tag{16}$$

where f is frequency in Hz.

Fig. 14a–c shows typical plots of Z'' vs. $1/f$ for the different cells at optimum applied potential window. The slope of these plots is equal to $(2\pi C_t)^{-1}$. The calculated capacitance values at 0.8 V for both symmetric PPy/PPy and SDPA/SDPA supercapacitors are 89 and 100.5 F g^{-1}, respectively. At 1.3 V for the hybrid PPy/SDPA supercapacitor a value of 96.5 F g^{-1} was obtained. These values are consistent with the results obtained from the charge–discharge experiments.

Table 3
Electrical parameters for both symmetric and the hybrid supercapacitor PPy/SDPA at different working potential window (V) evaluated from EIS test.

Cell	Working potential window (V)	R_{ct1} (Ω)	R_{ct2} (Ω) × 10^3	C_1 (F cm^{-2}) × 10^{-3}	C_2 (F cm^{-2}) × 10^{-1}
PPy/PPy	0.0	2.25	1.29	1.62	4.12
	0.3	1.94	1.01	2.04	4.36
	0.5	1.62	0.79	2.21	4.50
	0.7	1.40	0.60	2.52	4.88
	0.8	1.19	0.45	2.89	5.12
SDPA/SDPA	0.0	1.65	2.11	1.57	4.15
	0.3	1.54	1.57	1.84	4.31
	0.5	1.46	1.49	2.05	4.57
	0.7	1.25	1.24	2.31	4.62
	0.8	1.03	0.94	2.64	5.56
PPy/SDPA	0.0	1.69	2.99	1.93	3.88
	0.75	1.46	1.68	2.19	4.16
	1.0	1.26	0.83	2.44	4.66
	1.3	0.99	0.56	2.77	5.37
	1.5	1.98	1.82	1.61	3.03

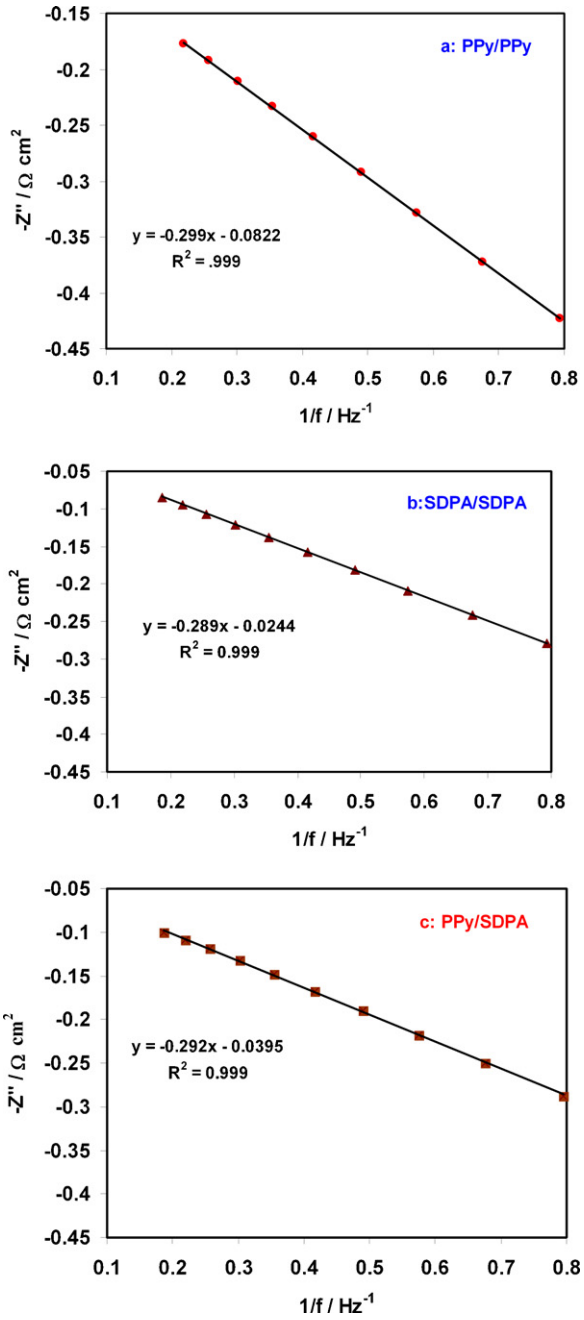

Fig. 14. Variation of imaginary component of impedance ($-Z''$) with the reciprocal of frequency ($1/f$) for both symmetric PPy/PPy and SDPA/SDPA supercapacitors and the hybrid PPy/SDPA cell. Points denote the experimental data while the line is obtained from the linear regression analysis.

4. Conclusion

Nanostructured SDPA and PPy were prepared by the controlled electrochemical oxidation of their monomers in aqueous media. The SDPA has good electroactivity at a mild pH, and its degradation is minimal compared with PAN. By employing modified GO with PPy and SDPA nanofibers as negative and positive electrodes, respectively, we broadened the working potential window of the hybrid PPy/SDPA supercapacitor in aqueous media up to 1.3 V, which is 1.6 times higher than the values obtained for both symmetric (PPy/PPy and SDPA/SDPA) configurations. Oxygen removal results in higher energy density (2.5 times the symmetric configuration) and a longer cycle life than has been previously reported for this system. Moreover, P_{max} of the hybrid PPy/SDPA system shows an improvement of more than 3-fold over the symmetric PPy/PPy supercapacitor and an improvement of more than 2-fold for the symmetric SDPA/SDPA supercapacitor. Based on the obtained results, the specific capacitance of 97 F g^{-1}, specific energy of 22.87 W kg^{-1} and specific power of 570 W kg^{-1} were calculated, which show improvements when compared with previous reports.

Acknowledgement

The support of the Tarbiat Modares University Research Council is gratefully acknowledged.

Appendix A. Supplementary data

Supplementary data associated with this article can be found, in the online version, at http://dx.doi.org/10.1016/j.electacta.2012.05.139.

References

[1] D.I. Gittins, D. Bethell, D.J. Schiffrin, R.J. Nichols, Nature 408 (2000) 67.
[2] R. Valiev, Nature 419 (2002) 887.
[3] C.J. Liu, U. Burghaus, F. Besenbacher, Z.L. Wang, ACS Nano 4 (2010) 5517.
[4] M.F. Mousavi, S. Ghasemi, Sonochemistry: A Suitable Method for Synthesis of Nano-structured Materials, Nova Science Publishers, Hauppauge, NY, 2010.
[5] M. Kiani, M. Mousavi, M. Rahmanifar, International Journal of Electrochemical Science 6 (2011) 2581.
[6] H.R. Ghenaatian, M.F. Mousavi, S.H. Kazemi, M. Shamsipur, Synthetic Metals 159 (2009) 1717.
[7] M.A. Kiani, M.F. Mousavi, S. Ghasemi, Journal of Power Sources 195 (2010) 5794.
[8] M. Inagaki, H. Konno, O. Tanaike, Journal of Power Sources 195 (2010) 7880.
[9] M.W. Xu, W. Jia, S.J. Bao, Z. Su, B. Dong, Electrochimica Acta 55 (2010) 5117.
[10] S.I. Cho, S.B. Lee, Dekker Encyclopedia of Nanoscience and Nanotechnology (2005) 1.
[11] F. Marchioni, J. Yang, W. Walker, F. Wudl, Journal of Physical Chemistry B 110 (2006) 22202.
[12] D. Reyman, E. Guereca, P. Herrasti, Ultrasonics Sonochemistry 14 (2007) 653.
[13] A.K. Bakhshi, G. Bhalla, Journal of Scientific and Industrial Research 63 (2004) 715.
[14] W. Sun, R. Zheng, X. Chen, Journal of Power Sources 195 (2010) 7120.
[15] V. Gupta, N. Miura, Materials Letters 60 (2006) 1466.
[16] Y.Y. Horng, Y.C. Lu, Y.K. Hsu, C.C. Chen, L.C. Chen, K.H. Chen, Journal of Power Sources 195 (2010) 4418.
[17] S. Bhadra, D. Khastgir, N.K. Singha, J.H. Lee, Progress in Polymer Science 34 (2009) 783.
[18] E. Frackowiak, V. Khomenko, K. Jurewicz, K. Lota, F. Béguin, Journal of Power Sources 153 (2006) 413.
[19] M. Selvakumar, S. Pitchumani, Korean Journal of Chemical Engineering 27 (2010) 977.
[20] A.A. Karyakin, I.A. Maltsev, L.V. Lukachova, Journal of Electroanalytical Chemistry 402 (1996) 217.
[21] A.A. Karyakin, A.K. Strakhova, A.K. Yatsimirsky, Journal of Electroanalytical Chemistry 371 (1994) 259.
[22] J. Li, F. Gao, Journal of Power Sources 194 (2009) 1184.
[23] A.L.M. Reddy, S. Ramaprabhu, Journal of Physical Chemistry C 111 (2007) 7727.
[24] S.B. Tang, M.O. Lai, L. Lu, Materials Chemistry and Physics 111 (2008) 149.
[25] K. Naoi, S. Ishimoto, Y. Isobe, S. Aoyagi, Journal of Power Sources 195 (2010) 6250.
[26] J.Y. Luo, Y.Y. Xia, Journal of Power Sources 186 (2009) 224.
[27] V. Ganesh, S. Pitchumani, V. Lakshminarayanan, Journal of Power Sources 158 (2006) 1523.
[28] R. Kötz, M. Carlen, Electrochimica Acta 45 (2000) 2483.
[29] V. Khomenko, E. Raymundo-Piñero, F. Béguin, Journal of Power Sources 195 (2010) 4234.
[30] X. Yang, T. Dai, Z. Zhu, Y. Lu, Polymer 48 (2007) 4021.
[31] S.I. Cho, S.B. Lee, Accounts of Chemical Research 41 (2008) 699.
[32] M.S. Rahmanifar, M.F. Mousavi, M. Shamsipur, Journal of Power Sources 110 (2002) 229.
[33] K. Ghanbari, M.F. Mousavi, M. Shamsipur, H. Karami, Journal of Power Sources 170 (2007) 513.
[34] H. Karami, M.F. Mousavi, M. Shamsipur, Journal of Power Sources 117 (2003) 255.
[35] H. Karami, M.F. Mousavi, M. Shamsipur, Journal of Power Sources 124 (2003) 303.
[36] H. Karami, M.F. Mousavi, M. Shamsipur, S. Riahi, Journal of Power Sources 154 (2006) 298.
[37] K. Ghanbari, M.F. Mousavi, M. Shamsipur, Electrochimica Acta 52 (2006) 1514.

[38] M.S. Rahmanifar, M.F. Mousavi, M. Shamsipur, H. Heli, Synthetic Metals 155 (2005) 480.
[39] Y. Han, Y. Lu, Carbon 45 (2007) 2394.
[40] K. Zhang, L.L. Zhang, X.S. Zhao, J. Wu, Chemistry of Materials 22 (2010) 1392.
[41] P. Novak, K. Muller, K.S.V. Santhanam, O. Haas, Chemical Reviews 97 (1997) 207.
[42] T. Brousse, P.L. Taberna, O. Crosnier, R. Dugas, P. Guillemet, Y. Scudeller, Y. Zhou, F. Favier, D. Bélanger, P. Simon, Journal of Power Sources 173 (2007) 633.
[43] V. Khomenko, E. Frackowiak, F. Béguin, Electrochimica Acta 50 (2005) 2499.
[44] J. Yan, T. Wei, Z. Fan, W. Qian, M. Zhang, X. Shen, F. Wei, Journal of Power Sources 195 (2010) 3041.
[45] V. Khomenko, E. Raymundo-Piñero, F. Béguin, Journal of Power Sources 153 (2006) 183.
[46] D.W. Wang, F. Li, H.-M. Cheng, Journal of Power Sources 185 (2008) 1563.
[47] S.B. Ma, K.W. Nam, W.S. Yoon, X.Q. Yang, K.Y. Ahn, K.H. Oh, K.B. Kim, Electrochemistry Communications 9 (2007) 2807.
[48] X. Liu, P.G. Pickup, Journal of Power Sources 176 (2008) 410.
[49] T. Cottineau, M. Toupin, T. Delahaye, T. Brousse, D. Bélanger, Applied Physics A-Materials Science & Processing 82 (2006) 599.
[50] H. Mi, X. Zhang, S. Yang, X. Ye, J. Luo, Materials Chemistry and Physics 112 (2008) 127.
[51] G.A. Snook, P. Kao, A.S. Best, Journal of Power Sources 196 (2011) 1.
[52] M.E. Orazem, B. Tribollet, Electrochemical Impedance Spectroscopy, Wiley, Hoboken, NJ, 2008.
[53] T.C. Girija, M.V. Sangaranarayanan, Synthetic Metals 156 (2006) 244.